New Pyrazole- and Benzimidazole-derived Ligand Systems

Mohammad Nozari,[a*] Anthony W. Addison,[a*] GorDan T. Reeves,[b] Matthias Zeller,[c] Jerry P. Jasinski,[d] Manpreet Kaur,[d] Jayakumar G. Gilbert,[e] Clifton R. Hamilton,[e] Jonathan M. Popovitch,[a†] Lawrence M. Wolf,[a†] Lindsay E. Crist,[a†] and Natalia Bastida[a]

[a]Department of Chemistry, Drexel University, 3141 Chestnut Street, Philadelphia, Pennsylvania 19104, USA
[b]Department of Chemistry, Stockton University, 101 Vera King Farris Drive, Galloway, New Jersey 08205, USA
[c]Department of Chemistry, Youngstown State University, One University Plaza, Youngstown, Ohio 44555, USA
[d]Department of Chemistry, Keene State College, 229 Main Street, Keene, New Hampshire 03435, USA
[e]Department of Chemistry, Temple University, 1901 N. 13th St, Philadelphia, Pennsylvania 19122, USA
*E-mail: mn468@drexel.edu; addisona@drexel.edu

Received August 17, 2017
DOI 10.1002/jhet.3155
Published online 00 Month 2018 in Wiley Online Library (wileyonlinelibrary.com).

†Work performed in partial fulfillment of the requirements for the Drexel University baccalaureate degree.

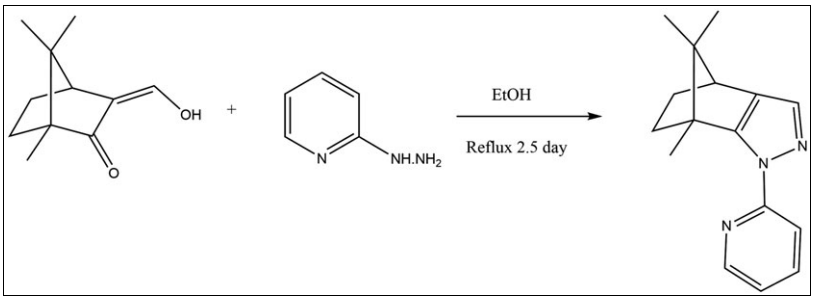

A series of *N*-containing heterocyclic compounds have been synthesized using approaches such as the well-known Knorr synthesis, and a facile *N*-alkylation method. This series of compounds includes pyrazole derivatives, tris(2-benzimidazolylmethyl)amine derivatives, and "pincer" ligands. Characterization methods include ^{1}H NMR, FT-IR, CHN analyses, UV-vis spectroscopy, and fluorimetry, while X-ray crystal structures are reported for most of the compounds. The crystallographic results affirm a ^{13}C NMR method for isomer assignment of substituted pyrazoles.

J. Heterocyclic Chem., **00,** 00 (2018).

INTRODUCTION

Transition metal ions play an important role in the physical and the chemical properties of enzymes [1]. The structural characterization of such enzymes has provided insight in understanding the type of donor groups that are bonded to the transition metal ions [2]. Among these donor groups, histidine imidazole donors are found in a wide variety of metalloenzymes [3]. Among other applications, nitrogen-containing compounds can be used as sensors for detecting toxic benzene metabolites [4]. One of the important factors in selective structuring of complexes' architecture is the hydrogen bonding capability of the ligands. These ligands provide available hydrogens and are also suitable candidates for selective complexation [5]. Ligands that incorporate pyridyl, benzimidazolyl, quinolyl, and indazole groups in their framework have had frequent applications due to their relative ease of synthesis and the ready incorporation of steric constraints [6–11]. Pyrazole derivatives, especially pyrazoles substituted with *N*-containing heterocycles, have been reported to exhibit antitumor [12–16] and antifungal properties [17,18], while benzimidazole and pyrazole moieties are among the most frequently used ring systems for small molecule drugs listed by the US FDA [19].

The tridentate ligand tris(2-benzimidazolylmethyl)amine (NTB) and its alkyl-substituted derivatives tris(*N*-R-benzimidazol-2-ylmethyl)amine (R = methyl, Me_3NTB; R = ethyl, Et_3NTB; R = propyl, Pr_3NTB) can form both mononuclear and multinuclear complexes, which have long been studied as models for metalloenzyme active sites [20–22] and more recently for their role in water electro-oxidation catalysis (with long-chain *N*-substituents) [23], photoluminescence of lanthanide complexes such as those of Sm^{3+}, Eu^{3+} and Tb^{3+}, Yb^{3+} [24,25], and DNA binding properties of Zn and Ni complexes [26]. A recent study on a ternary Fe(III) complex has shown that the complex binds to DNA *via* an intercalation binding mode [27]. Rhenium(I) complexes of imidazole derivatives have been used for electrocatalytic CO_2 reduction [28]. Imidazole-copper-based catalysts have recently been studied for application in lowering water oxidation overpotentials [29].

RESULTS AND DISCUSSION

Here, we report the synthesis and characterization of a diverse group of heterocyclic ligands (Figs. 1 and 2). For ligands **1–4**, a Knorr-type reaction is used to convert heterocyclic hydrazines and 1,3-dicarbonyl derivatives to substituted pyrazole compounds. The hydrazine derivatives utilized were 2-hydrazinoquinoline and 2-hydrazinopyridine. Typical Knorr reactions are initiated by imine (hydrazone) formation, the hydrazone derivatives then attack the second carbonyl group, resulting in a diimine. Deprotonation of the diimine delivers the pyrazole compound, while protonation of the initial carbonyl makes it more susceptible to attack by a nucleophilic group [30].

To obtain the ligand **1**, 2-benzoylcyclohexanone and 2-hydrazinoquinoline were refluxed in ethanol for 24 h**.** Because there are two possible sites for hydrazine nucleophilic attack with nonsymmetric diketones, we have to consider two isomer possibilities (Fig. 3). A

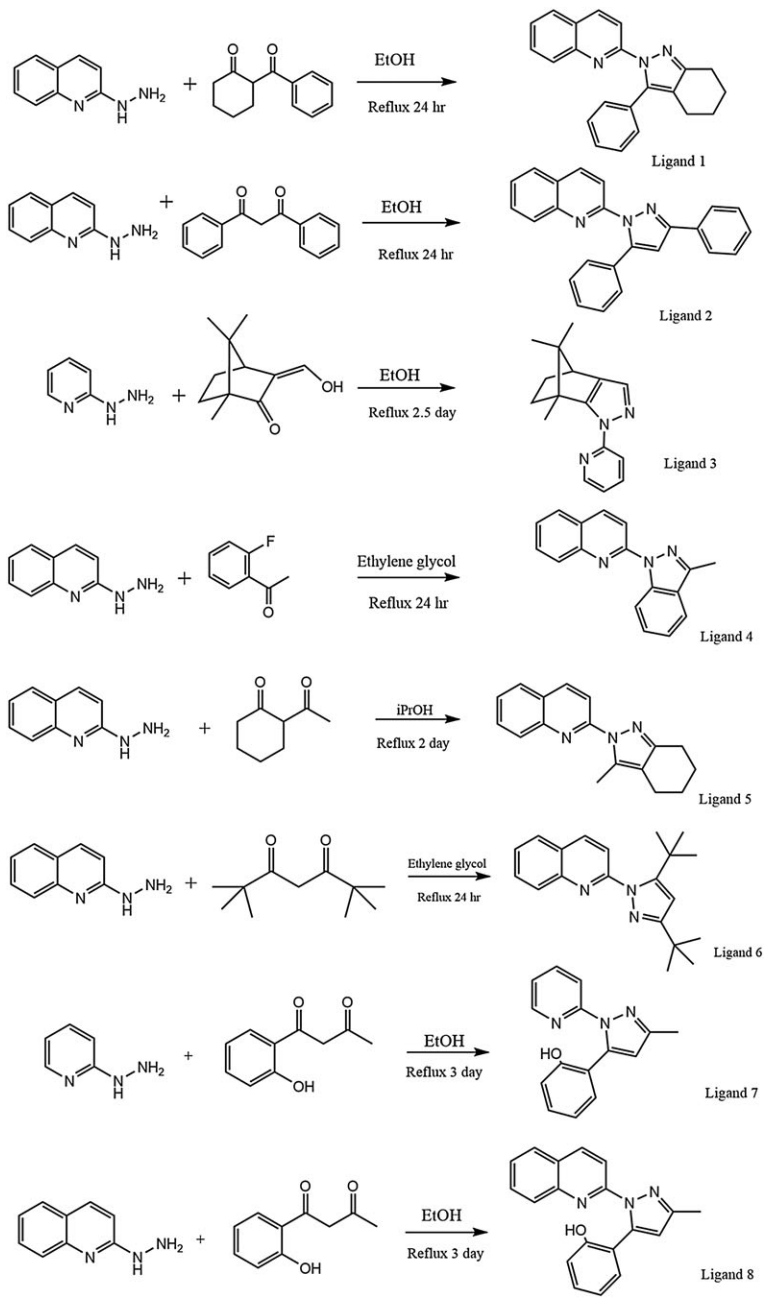

Figure 1. Knorr condensation reactions.

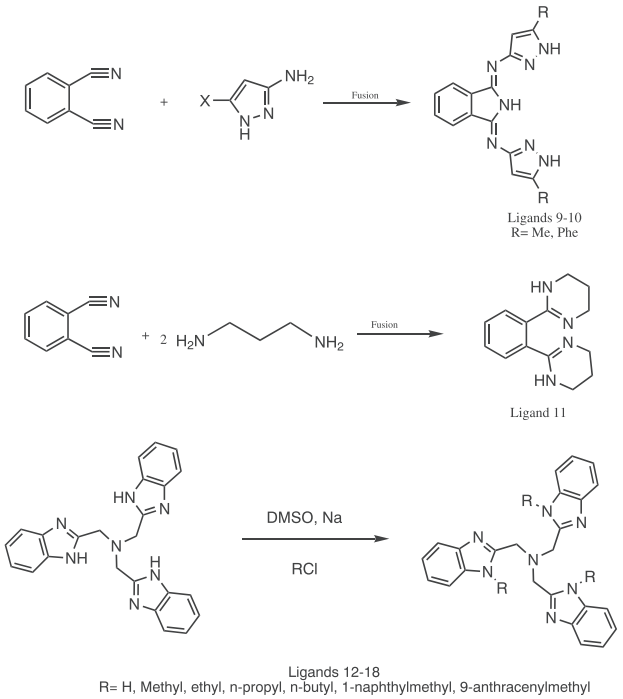

Figure 2. Heterocyclic ligands via nitrile-based condensations and N-alkylations.

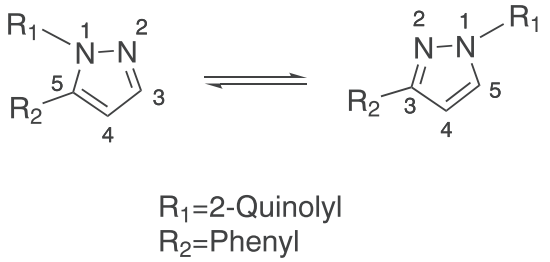

Figure 3. Two possible isomers for pyrazoles derived from nonsymmetric diketones.

similar pyrazole isomerism has been investigated, where the different isomers were isolated and proton and carbon atoms of the substituent groups were assigned by NMR [31–33]. It has been reported that 3-aryl substituent positioning is preferred over 5-aryl substitution [31]; however, exceptions have been observed whereby internal H-bonding has promoted the 5-aryl substituent [31]. Singh *et al*. have reported larger values of δ C4 ^{13}C NMR chemical shift for a 3-aryl substituent than a 5-aryl substituent (δ C4:103.8, 108.3, respectively) [32], while in our case, the δ C4 chemical shift is 109.2 (Fig. S15). In a comparison of chemical shifts for C3 and C5, Catalan *et al*. [31] demonstrated that whichever of C3 or C5 is aryl substituted possesses the larger ^{13}C chemical shift value, and this further supports our assignment. In addition, ^{13}C NMR evidences the existence of only one isomer in the bulk product, as the number of resonances observed in the spectrum corresponds to the number of carbon atoms in the product.

The X-ray structure obtained (Fig. 4) confirms the 5-aryl substituted version's formation. Crystal and refinement X-ray data are presented in Tables 1A and 1B.

The ligand-**1** molecule is not overall planar, the angles formed between the phenyl- and quinoline-containing planes with the pyrazole plane in the molecule are 36.6° and 38.8°. When the molecule is viewed along the pyrazole plane with the cyclohexenyl group at the front, then the enantiomers within the unit cell of **1** may be distinguished by the twist of the quinolyl group versus the pyrazole plane: clockwise in one case, anticlockwise in the other. In ^{1}H NMR, the chemical shifts for quinoline, phenyl, and cyclohexane protons are well resolved at (8.46, 8.02), (7.63, 7.18), and (2.83, 1.84) ppm, respectively. Similar results are observed for our other ligands with analogous structures. The IR spectrum displayed absorption bands at ν_{max} = 2926, 3061, 1616, and 1598 cm^{-1} characteristic bands for sp^3 CH, sp^2 CH, C═N, and C═C vibrations, respectively, the last three of which are in the range previously reported for pyrazoles [34].

Ligand **2** (Fig. 5) was synthesized using the same technique as for **1**, but with more extensive reflux and using dibenzoylmethane as the dicarbonyl compound. The ^{1}H NMR shows chemical shifts for quinoline, phenyl, and pyrazole protons at 8.10, (7.84, 7.50, and 7.35), and 6.9 ppm, respectively. Ligand **2** displays an IR spectrum similar to that of ligand **1**.

The quinolyl, pyrazolyl, and 3-phenyl groups form a bowed plane, the bowing being a contributor to the inter-

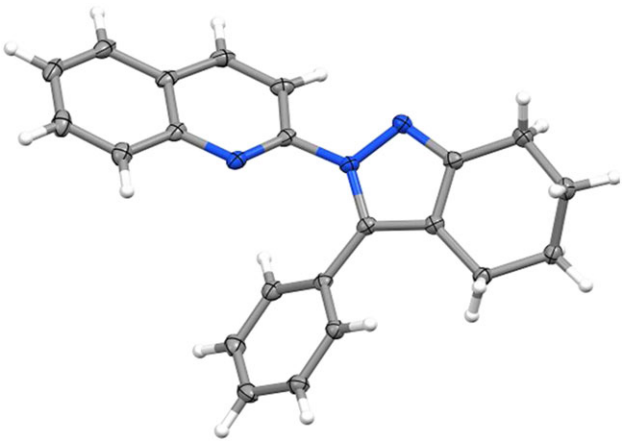

Figure 4. ORTEP structure of the bidentate quinolyl–tetrahydroindazole ligand **1**. For this and all subsequent ORTEP diagrams, the nonhydrogen atoms are rendered as 50% probability ellipsoids, and H atoms are rendered as spheres of arbitrary radius. Other structural views of this and succeeding molecules are in Figures S1–S13. [Color figure can be viewed at wileyonlinelibrary.com]

Table 1A

Crystal data for compounds **1–6**.

Compound	Ligand 1	Ligand 2	Ligand 2 intermediate	Ligand 3	Ligand 4	Ligand 5	Ligand 6
Empirical formula[a]	$C_{22}H_{19}N_3$	$C_{24}H_{17}N_3$	$C_{24}H_{19}N_3O$	$C_{16}H_{19}N_3$	$C_{17}H_{13}N_3$	$C_{17}H_{17}N_3$	$C_{21}H_{29}N_3O$
Formula wt.	325.40	347.41	365.42	253.34	259.3	263.33	339.47
Temperature (K)	100(2)	100(2)	100(2)	100(2)	269(2)	173(2)	100(2)
Wavelength (Å)	0.71073	0.71073	0.71073	0.71073	0.71073	1.54184	0.71073
Crystal system	Triclinic	Monoclinic	Monoclinic	Orthorhombic	Monoclinic	Monoclinic	Orthorhombic
Space group	$P\bar{1}$	C2	C2/c	$P2_12_12_1$	$P2_1/n$	$P2_1/n$	$Pca2_1$
Unit cell dimensions							
a (Å)	8.528(10)	26.610(7)	30.452(3)	6.9806(4)	7.4320(7)	12.8553(4)	21.5014(8)
b (Å)	11.943(13)	5.9750(16)	7.9201(9)	12.2510(7)	10.9216(10)	7.4279(2)	8.6745(3)
c (Å)	17.428(18)	11.429(3)	16.5073(17)	15.7231(9)	15.6584(14)	14.2872(4)	10.3573(4)
α (deg)	91.49(3)	90	90	90	90	90	90
β (deg)	100.84(2)	108.513(5)	113.549(2)	90	91.0200(10)	100.698(3)	90
γ (deg)	110.37(2)	90	90	90	90	90	90
Volume ($Å^3$)	1626(3)	1723.1(8)	3649.71 (6)	1344.63(13)	1270.8(2)	1340.54(7)	1931.78(12)
Z	4	**4**	8	4	4	4	4
ρ_{calcd} (g/cm^3)	1.329	1.339	1.331	1.252	1.315	1.305	1.167
Absorption coeff. (mm^{-1})	0.080	0.080	0.083	0.076	0.083	0.614	0.073
F(000)	726	728	1536	544	544	560	736
θ range for data collection (deg.)	1.20 to 28.60	1.71 to 28.11	1.46 to 28.28	2.59 to 30.45	2.27 to 31.80	3.46 to 71.36	2.73 to 30.49
wR_2 ($I > 2\sigma_I$)	0.097	0.080	0.106	0.014	0.103	0.117	0.146

[a]Empirical formula includes lattice solvation.

Table 1B

Crystal data for compounds **7–17**.

Compound	Ligand 7	Ligand 8	Ligand 9	Ligand 10	Ligand 16	Ligand 17
Empirical formula	$C_{15}H_{15}N_3O_2$	$C_{19}H_{17}N_3O_2$	$C_{31}H_{30}N_8O_2$	$C_{16}H_{15}N_7$	$C_{36}H_{45}N_7$	$C_{57}H_{45}N_7$
Formula wt.	269.3	319.35	546.63	430.2	575.9	828
Temperature (K)	100(2)	100(2)	100(2)	100(2)	173(2)	173(2)
Wavelength (Å)	0.71073	0.71073	0.7103	0.7103	0.71073	1.54184
Crystal system	Monoclinic	Monoclinic	Monoclinic	Monoclinic	Trigonal	Monoclinic
Space group	$P2_1/c$	$P2_1/c$	$P2_1/c$	$P2_1/c$	$R\bar{3}$	$P2_1/n$
Unit cell dimensions						
a (Å)	14.0879(17)	16.0994(7)	8.4620(8)	10.1047(16)	17.2984(7)	9.2351(2)
b (Å)	6.9688(8)	7.1114(3)	27.162(3)	17.237(3)	17.2984(7)	32.4366(6)
c (Å)	14.4283(17)	14.1519(6)	11.6827(11)	9.5700(15)	18.7912(9)	14.4513(3)
α (deg)	90	90	90	90	90	90
β (deg)	199.482(2)	107.1234(16)	94.8120(10)	116.726(2)	90	95.405(2)
γ (deg)	90	90	90	90	120	90
Volume ($Å^3$)	1335.4(3)	1548.42(12)	2675.8(4)	1488.78	4869.6(5)	4309.71(15)
Z	4	4	4	4	6	4
ρ_{calcd} (g/cm^3)	1.339	1.37	1.357	1.254	1.178	1.276
Absorption coeff. (mm^{-1})	0.092	0.091	0.089	0.088	0.552	0.591
F(000)	568	672	1152	986	1860	1744
θ range for data collection (deg.)	2.87 to 31.84	2.64 to 30.51	2.30 to 31.03	2.43 to 32.851	3.77 to 71.02	3.36 to 71.28
wR_2 ($I > 2\sigma_I$)	0.112	0.127	0.117	0.130	0.043	0.072

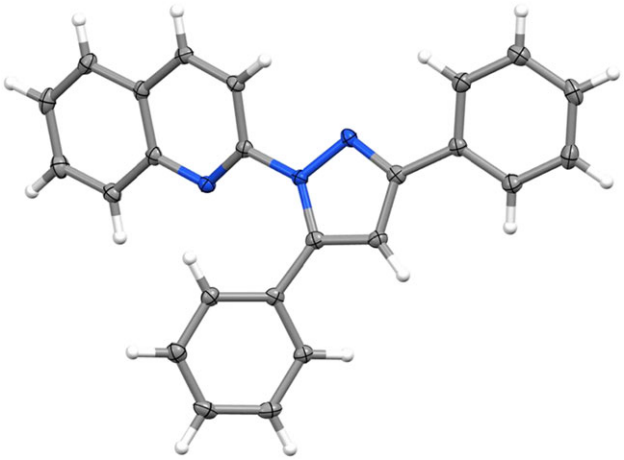

Figure 5. ORTEP structure of the bidentate quinolyl–pyrazole ligand **2**. [Color figure can be viewed at wileyonlinelibrary.com]

ring angles (16.6° for the phenyl group, 22.7° for the quinolyl group, *vs*. the pyrazole ring) (Fig. 5). The handedness of rotation of the 5-phenyl group (34.5° vs. the pyrazole) with respect to the bowed plane is presumably the source of chirality of the unit cells, this compound being an example of conglomerate crystallization (spontaneous resolution) [35]. The molecules are arrayed roughly parallel to the *b*-direction (the quinoline rings are tipped by 21° to it). The 5-phenyl rings of one array are interdigitated between the quinoline rings of molecules of the adjacent array, with the arraying and interdigitation alternating in direction, but there is no π-π stacking.

With shorter refluxing (12 h in EtOH) of the reactants, dehydration of the diamine is incomplete, leaving a hydroxyl group on the molecule. This intermediate pyrazoline has also been isolated and defined by its X-ray structure (Fig. 6).

The OH group on the central ring in the intermediate causes the two phenyl rings to twist more toward each other, the angle between the two phenyl rings being 26.4° in the final product, while it is 100.0° in the intermediate. The potential role of the 5-phenyl group's rotation in individual molecule chirality is presumably overshadowed by the stereochemistry of the pyrazoline C5 itself. In the intermediate, several interactions are observed between the OH hydrogen and the quinoline nitrogen within the same molecule (O─H···N is 2.24 Å), and oxygen of OH and two hydrogens on the adjacent quinoline molecule (C─H···O: 2.50, 2.66 Å), these interactions being attributed to H-bonding. The pyridine ring planes are aligned parallel to the *a*-direction.

Formation of ligand **3** was a rather slow reaction at reflux in EtOH, requiring that 3-(hydroxymethylene)camphor and 2-hydrazinopyridine be refluxed for 2.5 days. The keto-enol tautomerism of 3-(hydroxymethylene)camphor has been

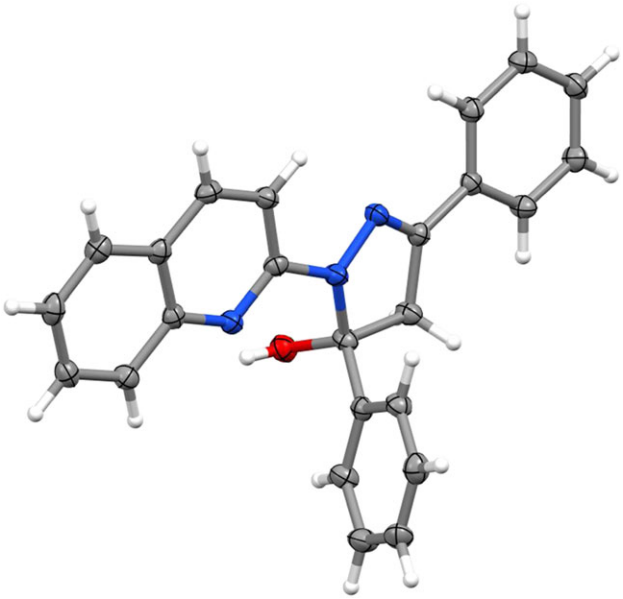

Figure 6. ORTEP structure of ligand **2** intermediate, the hydroxypyrazoline. [Color figure can be viewed at wileyonlinelibrary.com]

explored both in solution and in the solid state [36]; for 3-(hydroxymethylene)camphor, the condensation can be envisioned as proceeding *via* the diketone to form the hydrazone and then the pyrazole. This ligand contains CH, CH_2, and CH_3 groups that are observed in ^{1}H NMR at 7.48, 1.92, and 0.96 ppm, respectively. In the IR spectrum characteristic bands at 3054 cm^{-1} (ν sp^3 CH), 2953 cm^{-1} (ν sp^2 CH), 1611 cm^{-1}, and 1592 cm^{-1} are observed. This chiral compound was characterized by X-ray crystallography (Fig. 7), circular dichroism (CD) (Fig. 8), and optical rotation. There are four molecules of equivalent symmetry in the $P2_12_12_1$ unit cell, one of the space groups associated with intrinsically chiral structures.

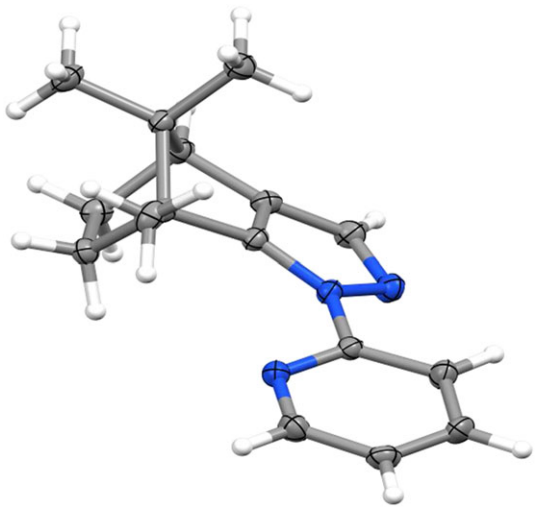

Figure 7. ORTEP structure of the chiral pyridyl–pyrazole ligand **3**. [Color figure can be viewed at wileyonlinelibrary.com]

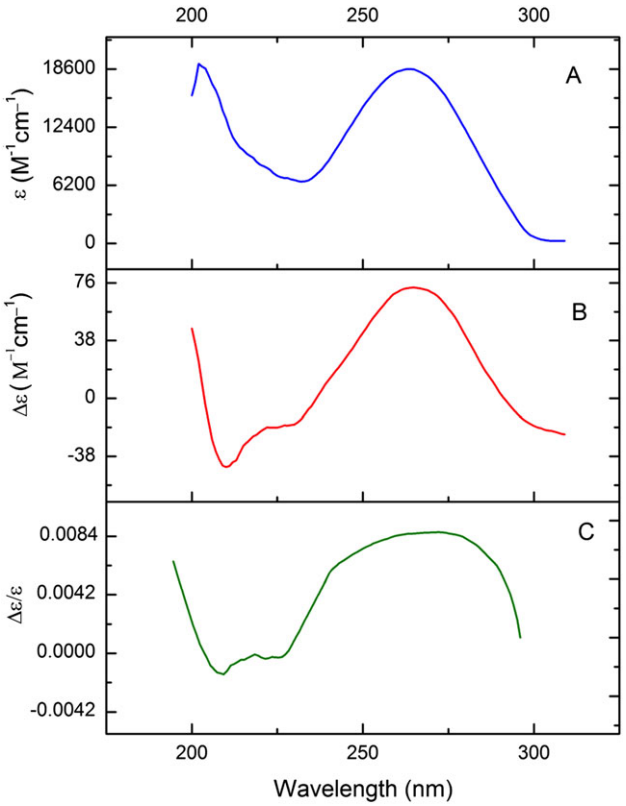

Figure 8. A: UV absorption spectrum of 79 μM ligand **3** in acetonitrile. B: The UV-CD spectrum of the ligand **3** solution. C: Kuhn anisotropy spectrum of the compound. [Color figure can be viewed at wileyonlinelibrary.com]

The pyridine plane is twisted 25.3° away from the pyrazole plane. The compound has a positive specific rotation $[\alpha]_D^{20}$ = +13.8 deg cm^{-2} g^{-1} (0.025 g/100 mL, CH_3CN). The UV-CD spectrum of ligand **3** displays a positive Cotton effect at λ_{max} = 261 nm, with a broad Kuhn anisotropy of *ca*. +0.0086–+0.0089 in the longest-wavelength absorption region, consistent with the optical rotation's sign.

Ligand **4** was prepared by a rather different approach, using 2′-fluoroacetophenone instead of a dicarbonyl. Initial condensation of the hydrazine NH_2 group with the ketone carbonyl group is followed by nucleophilic attack of the second nitrogen on the fluorine-bonded carbon, so that fluoride acts as a leaving group, resulting in generation of protonated ligand **4**. There are four symmetry-equivalent molecules in the unit cell, (Fig. 9). The molecules are almost planar, the quinoline and pyrazole planes being twisted only 6.4° away from complete coplanarity. The molecules are head-to-tail π-stacked at 19° to the *a*-direction, with the quinoline & indazole rings 3.50 ± 0.12 Å apart.

The structure of the Knorr product pyrazole ligand **5** is analogous to that of ligand **4** except for the saturated ring, 2-acetylcyclohexanone being used as reactant with

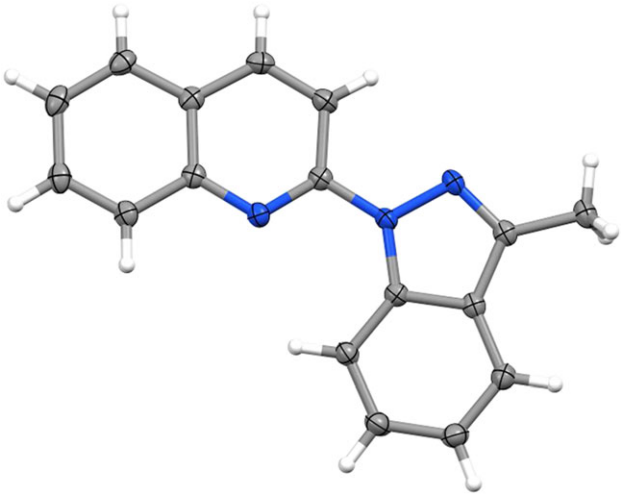

Figure 9. ORTEP structure of the quinolyl–indazole ligand **4**. [Color figure can be viewed at wileyonlinelibrary.com]

2-hydrazinoquinoline instead of 2′-fluoroacetophenone. Ligand **5** has a similar IR spectrum to ligand **4**, but in ^{1}H NMR, the distinctive chemical shifts are well-resolved for the quinoline protons at 8.22 (1 H, d), 8.09(1 H, d), 7.90 (1 H, d), 7.80 (1 H, d), 7.68 (1 H, t), 7.48 (1 H, t) ppm, cyclohexane and methyl protons at 2.76 (4 H, m), 2.52 (2 H, t), 1.82 (5 H, m) ppm.

The X-ray structure of the compound (Fig. 10) reveals four symmetry-equivalent molecules in the monoclinic unit cell. The molecule is not planar overall, the quinoline and pyrazole planes being twisted 15.5° away from each other. The molecules are arrayed in two directions in the lattice, at 51° to one another, and putative stacking is at *ca*. 4.45 Å, because of the cyclohexenyl ring's saturation.

Some compounds are less reactive toward condensation under these conditions. For example, we attempted to prepare ligand **6** using the aforementioned techniques, however, after 2 days' reflux in EtOH, the desired product was not detected and the ring closure was incomplete.

Figure 10. ORTEP structure of the quinolyl–tetrahydroindazole ligand **5**. [Color figure can be viewed at wileyonlinelibrary.com]

Eventually, ligand **6** was successfully prepared using 2,2,6,6-tetramethyl-3,5-heptanedione and hydrazinoquinoline by refluxing in ethylene glycol for a period of 24 h. Two solvomorphs were obtained: crystallization from aqueous ethanol yielded monoclinic ($P2_1/c$) crystals; however, a better-quality structure ($Pca2_1$; Tables 1 and 2; Fig. 11) was obtained for crystals from methanol, incorporating solvating MeOH. Some π-π stacking interactions in the former case are replaced by stronger H-bonding interactions in this latter solvate.

Interactions are observed between the alcohol OH and N on pyrazole, (O─H···N is 2.08 Å), and O of OH and H on the quinoline (C─H···O is 2.65 Å). The molecule is not overall planar, with the quinoline and pyrazole planes turned 51.8° away from coplanarity. In the ^{1}H NMR, methyl protons are observed as singlets as 1.28 and 1.36 ppm, the C4 pyrazole proton at 6.28 ppm and quinoline protons at 8.08–7.68 ppm.

Salicyloylacetone (1-(2′-hydroxyphenyl)butane-1,3-dione) reacts with 2-hydrazinopyridine for 3 days under reflux in EtOH to yield ligand **7**. Unlike the cyclization of salicyloylacetone by loss of a water molecule and chromene formation [37], the phenolic OH group does not participate in the reaction and the carbonyl groups undergo only a cyclization with hydrazinopyridine. Of the two possible isomeric products (Fig. 12), the X-ray results evidence the dominant one as being the "A" isomer (Fig. 13), which is unsuitable as a tridentate chelating agent, although (N,N) or (N,O) bidentacy is feasible in a mononucleating situation. As in ligand **1** and ligand **5**, initial hydrazone formation has occurred at the alkyl-, rather than the aryl-substituted carbonyl [31]. A solvating water molecule can be seen in the structure (Fig. 13).

In **7**, there are H-bonding interactions between O of the water molecule and H on the hydroxyl group (O─H···O is 1.80 Å), and of the N of the pyrazole with H of the water molecule (O─H···N is 2.86 Å). Two molecules of each enantiomer are present in the unit cell (Fig. 13), their individual chirality again arising from ring twists versus one another. Relative to the pyrazole ring plane, the phenol and pyridine rings are both rotated clockwise (phenolic-O "up on left") in one enantiomer, anticlockwise (phenolic-O "down on left") in the other. The X-ray structure also shows that the pyridyl and phenol planes are rotated by 53.7° and 56.2° versus the pyrazole plane, respectively. Alongside the typical pyrazole IR bands, a broad OH vibration is also observed at ν = 3400 cm^{-1} in the IR spectrum. Beside the distinctive CH and CH_3 proton shifts, the phenolic OH proton is observed as a singlet at 9.32 ppm in the NMR.

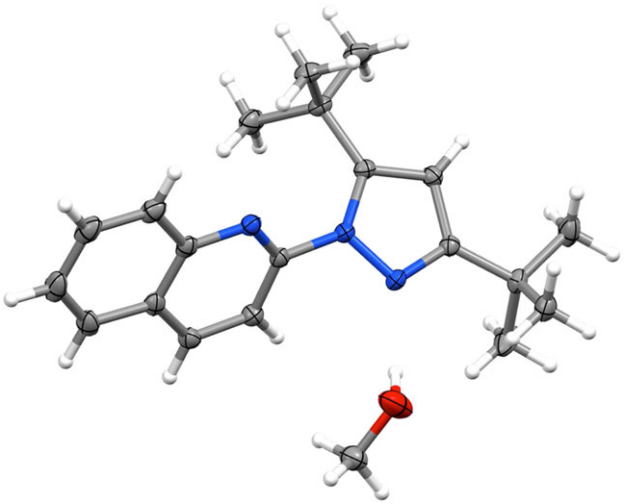

Figure 11. ORTEP structure of the quinolyl–pyrazole ligand **6**. [Color figure can be viewed at wileyonlinelibrary.com]

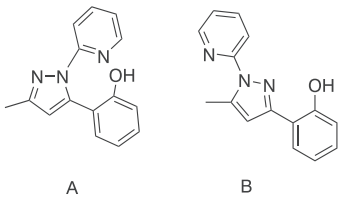

Figure 12. The two possible isomers for ligand **7**.

In a similar manner, salicyloylacetone reacts with 2-hydrazinoquinoline to produce ligand **8**. The X-ray structure of the compound (Fig. 14) shows that this molecule is again not planar overall; the quinoline and phenol planes are rotated by 49.1° and 47.5° versus the pyrazole plane, respectively. The individual molecule solid-state chirality is akin to that in ligand **7**, the nonpyrazole rings being concordantly rotated to be pseudo-parallel in either of the two directions. Along the crystallographic c-direction, π-π stacking of the quinoline rings is observed, with ring separations of 3.63 ± 0.03 Å.

Similarly to ligand **7**, there is a water of solvation in the structure of ligand **8**, with interactions observed between O of the water molecule and H on the hydroxyl group (O─H···O is 1.76 Å), and also between N of the pyrazole and the H of the water molecule (O─H···N is 2.90 Å). The IR spectrum displayed a characteristic broad OH vibration band at ν = 3350 cm^{-1}, while **8** has a similar ^{1}H NMR pattern to that of ligand **7**; the phenolic OH proton is observed at 9.22 ppm. As in the case of ligand **7**, this is the less-suited isomer for chelation, although in both cases, the compounds may act as anionic ligands *via* phenol deprotonation.

Tridentate **9** (Fig. 15) belongs to what has recently become known as the "pincer" type class of ligands, which are effective metal chelators whose coordination chemistry has long been studied. They have customarily been prepared by condensation of phthalonitrile with primary (aromatic) amines, as per Elvidge & Linstead's method [38] or Siegl's variation thereon [39], the latter

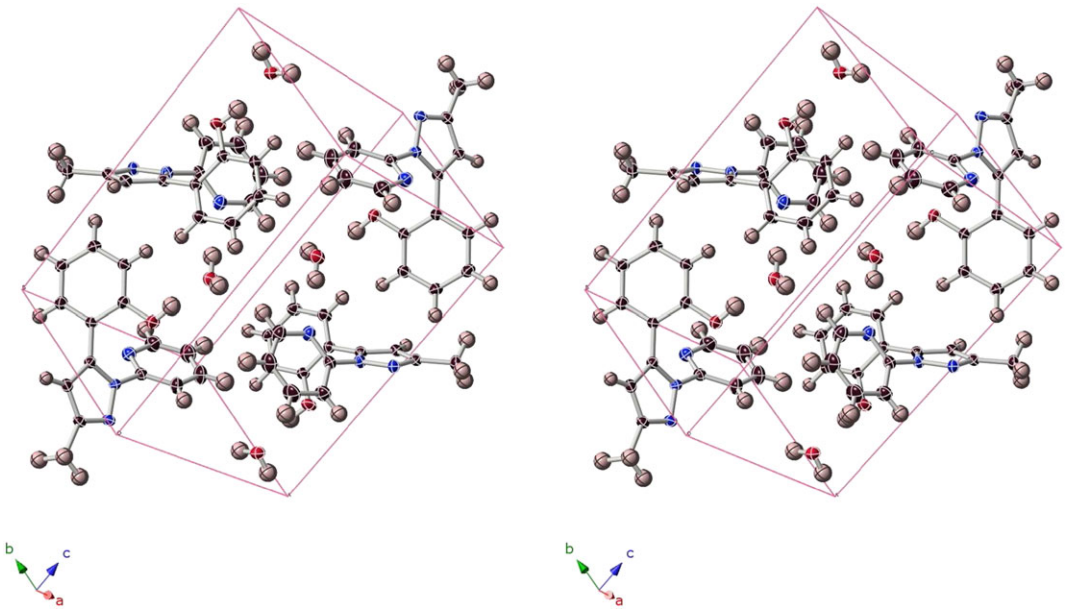

Figure 13. ORTEP rendering of the phenolic pyridyl–pyrazole ligand **7** unit cell, approximately along the *a*-direction; the upper left and lower right molecules, for instance, are enantiomers. (*CrystalMaker* 9, inverse stereoview, 75% probability ellipsoids). [Color figure can be viewed at wileyonlinelibrary.com]

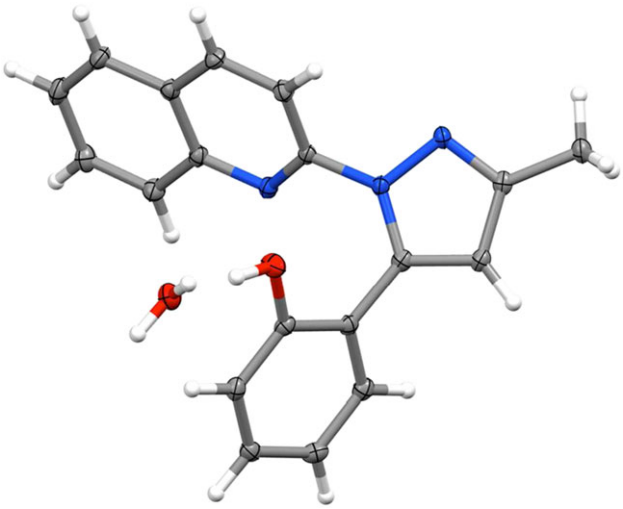

Figure 14. ORTEP structure of the phenolic quinolyl–pyrazole ligand **8**. [Color figure can be viewed at wileyonlinelibrary.com]

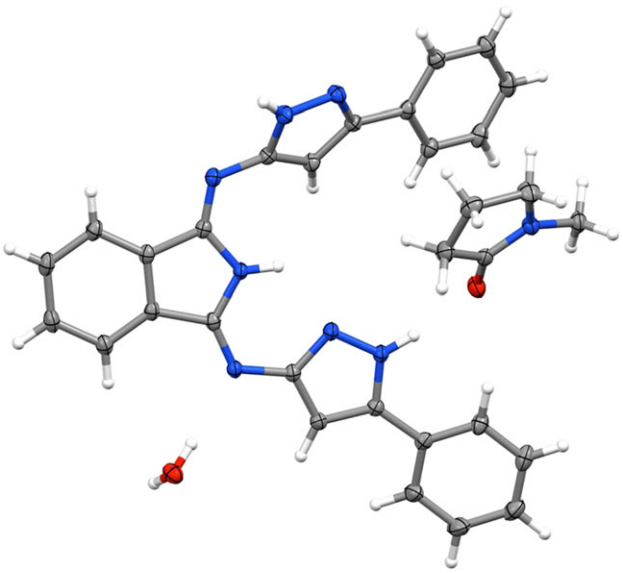

Figure 15. ORTEP structure of the phenylpyrazolyl–diiminoisoindoline ligand **9.** [Color figure can be viewed at wileyonlinelibrary.com]

using cationic promoters in an alcohol medium [39]. However, neither solvent nor promoter are necessary, as fusion of neat reactants is quite effective [6], this solventless fusion method requiring higher temperature (160–190°C), but being relatively quick. It is surmised that primary amine R-NH_2 undergoes nucleophilic addition across a phthalonitrile C═N linkage, leading to intramolecular cyclization with formation of an iminoisoindoline. This bears the R-group as the imine's N-substituent, and the addition of a second amine results in loss of ammonia and formation of the product [39]. For preparing ligand **9**, phthalonitrile was simply heated with 3-amino-5-phenylpyrazole. A microwave approach utilized a small amount of ethylene glycol as a microwave-absorbing solvent. The thermal solventless melt method nonetheless showed a higher yield, and was more reproducible than the microwave technique. The characteristic isoindoline NH vibration is observed in IR spectroscopy at ν = 3300 cm^{-1}; NH protons on pyrazole

and isoindoline are observed at δ 13.57 ppm (2H) and 6.81 ppm (1H) in the ^{1}H NMR.

The X-ray structure obtained for ligand **9** displays both an *N*-methylpyrrolidinone (NMP) and a water molecule of solvation, with H-bonding interactions observed between N of pyrazole and H of the water molecule (O─H···N is 2.11 Å) and also between O of the water molecule and H on the pyrazole (N─H···O is 2.85 Å), as well as between O of NMP and H on the pyrazole (N─H···O is 1.87 Å; Fig. 15). Indeed, recrystallization of the product from NMP occurred only after absorption of atmospheric water by the solution over a long period of time. None of the molecule's rings are coplanar. The terminal benzene planes are twisted 11.3° and 17.4° away from their adjacent pyrazole planes, which are in turn twisted 6.3° and 37.8° away from the isoindoline plane, in the opposite direction. The isoindoline-pyrazole(N1)-phenyl(C6) ring sets are almost coplanar, with consecutive but opposite twists of 5.3° and 11.3°. The solvating NMP appears to displace the N7/C21 arm so that a C17-N5-C18-C19 torsion of 37° (and like interplanar angle) twists this other phenylpyrazolyl arm further away from the isoindoline plane. The corresponding phenyl versus pyrazolyl twist is 17.4°, again conrotatory. Nor is the N5─C17 imine bond completely immune to these influences, being itself twisted by 5.8°. Nonetheless, a broader view of the molecule is that there is substantial planarity, although with one of the phenylpyrazolyl arms twisted away from the rest of the molecule, so that the two phenyl groups are at 32.4° to one another. The isoindoline moieties are stacked alternating head:tail roughly along an *ab* diagonal, with interplanar distances of 3.42 ± 0.02 Å, while the NMP are stacked against a ligand pyrazole, with the NMP ring atoms at 3.39 ± 0.11 Å from the pyrazole mean plane.

The pyrazolyl-isoindoline ligand **10** was also prepared using the fusion method; the pyrazole used in the synthesis was 3-amino-5-methyl-1*H*-pyrazole. Similarly, to ligand **9**, characteristic NH protons are observed at δ 12.50 ppm (2H) and 6.10 ppm in the NMR. The X-ray structure obtained (Fig. 16) confirms the nature of the product.

The pyrazole planes are twisted 25.9° and 4.8° away from coplanarity with the isoindoline plane, in an antiparallel sense. One of the methyl substituents is rotationally disordered between two positions. Viewed along the direction 0.9, 0.1, 2.25 (U, V, W), the molecules are seen edge-on, stacked in a herringbone pattern in the lattice. The stacking is again alternating, benzo-"head" to pyrrole "tail," with the interplanar distances between the isoindoline moieties' atoms ranging from 3.24 to 3.27 Å.

In another nitrile-based synthesis essay, the reaction of phthalonitrile with 1,3-diaminopropane, cyclization reactions

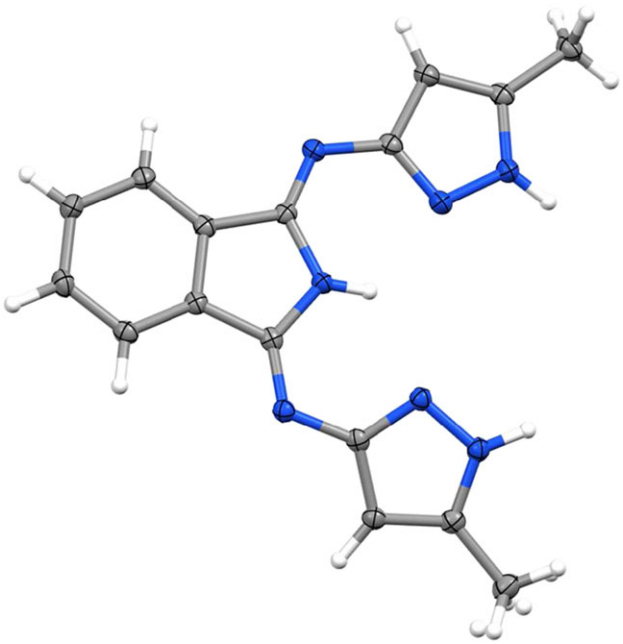

Figure 16. ORTEP structure of the methylpyrazolyl–diiminoisoindoline ligand **10**. [Color figure can be viewed at wileyonlinelibrary.com]

occur at each of the two nitriles and the bis(tetrahydropyrimidine) ligand (**11**) results. The IR spectrum displays a characteristic NH vibration at ν = 3255 cm^{-1}. CH, NH, and CH_2 protons are observed by ^{1}H NMR at 8.22, 7.90, and 3.42–2.62 ppm, respectively. This ligand is a homologue of the corresponding bis(imidazoline) described by Lever *et al*. [40].

N-alkylation of NTB, tris(benzimidazol-2-ylmethyl) amine, to obtain *N*-substituted derivatives, namely, Me_3NTB, Et_3NTB, Pr_3NTB, Bu_3NTB, Np_3NTB, and An_3NTB, utilized sodium metal in dimethyl sulfoxide (DMSO) for deprotonation of the labile NH units [41,42]. Past syntheses of related ligands have utilized (commercially available) *N*-methyl-*o*-phenylenediamine (for Me_3NTB) or similar N─H deprotonation with reagents and solvents that could nonetheless entail solvent reaction (acetone) or equilibrium deprotonation (KOH, alkoxides). NTB and Na were stirred under nitrogen with venting of the byproduct H_2 pressure, and after sodium dissolution and concomitant NTB deprotonation, alkyl halide was added, and the solution was stirred until any precipitation appeared to be complete. For isolation, the product was precipitated with water and filtered off or solvent-extracted (toluene or benzene) and ultimately recrystallized. However, this *N*-alkylation method was not successful with 2° or 3° alkyl halides, and the DMSO should be dry.

In Np_3NTB and Et_3NTB, for example, CH_2 groups exist in two different chemical environments, one of them connecting benzimidazole groups to the central N, and

the other connecting the aryl group to the nitrogen. These protons on different locations are distinctively observable at 5.65 and 4.32 ppm and shifted to approximately 1 ppm larger values than typical nonshifted CH_2 protons, as expected. X-ray crystal structures for Bu_3NTB and Np_3NTB (the naphthylmethyl derivative) ligands are illustrated by Figures 17 and 18, while Figure S10 shows a representation of an Et_3NTB structure. In all of these ligands, the conformation has the three benzimidazole arms directed "upward," toward the apex of the central aliphatic nitrogen's NC_3 trigonal pyramid. Metal coordination thus necessitates substantial swiveling of the benzimidazoles about their methylene links to the central N. The three benzimidazole planes can be envisioned as three blades of a propeller structure connected to the central N, as the benzimidazole arms are oriented at (different) angles of less than 45° versus the $N_{central}C_3$ pseudo-threefold axis. For Bu_3NTB and Np_3NTB, the individual molecule asymmetry arises in the immediacy from the tilt directions of the benzimidazole planes relative to that axis—forming a right-handed "propeller" in one case, and a left-handed one in the other. The average angle between the propellers is 67.1° in Np_3NTB, while in the case of Bu_3NTB, the propellers "blades" are oriented all at the same angle of 88.1° from each other. In the Bu_3NTB lattice, there is slightly sideways-slipped head-to-tail π-π stacking (3.48 ± 0.01 Å) between two benzimidazoles on adjacent molecules, while in Np_3NTB, these are replaced by naphthyl–naphthyl interactions (at 3.64 ± 0.02 Å). The

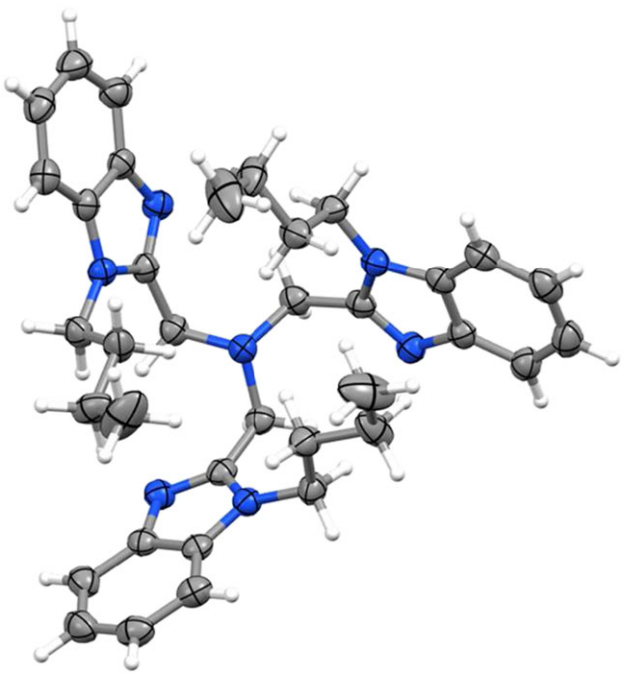

Figure 17. ORTEP structure of the *n*-butylated tripodal benzimidazole ligand **L16**. [Color figure can be viewed at wileyonlinelibrary.com]

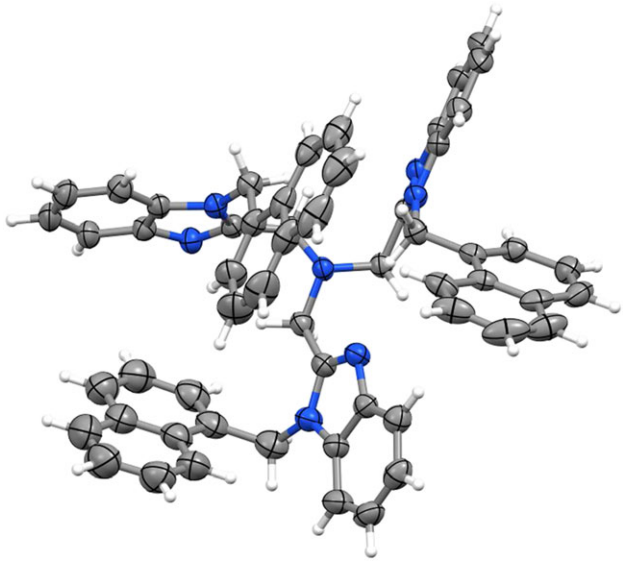

Figure 18. ORTEP structure of the naphthyl-derived tripodal benzimidazole ligand **L17**. [Color figure can be viewed at wileyonlinelibrary.com]

naphthyl plane is typically at about 78° versus its benzimidazole's plane.

UV absorption and fluorimetry. The optical absorption spectra of all the ligands were investigated and are summarized in Tables 2 and 3. The UV spectrum of ligand **5** (73.1 μM in acetonitrile) is displayed in Figure 19 as an example.

These pyrazole derivatives contain quinoline, pyrazole, benzene, and pyridine components, which are observable in the UV spectra. For instance, ligand **1** contains quinoline, pyrazole, and benzene motifs, the UV spectra of the compound displaying peaks with λ_{max} at 207, 241, 268, 285, 321, and 333 nm. Several of the observed bands can be assigned to π-π* transitions of the pyrazole (207 nm), benzene (241 nm), and quinoline (268, 285, 333 nm) moieties, respectively, similarly to those observed in previous studies [43,44].

Fluorescence characteristics of the ligands were also investigated. Figure 20 displays the excitation spectrum of a 1.2 μM solution of ligand **1** in acetonitrile, at ambient temperature.

With excitation wavelengths of 243 and 283 nm (π-π*) used for obtaining the emission spectrum, fluorescence emission by **1** was observed at 342 nm, which we associate with excitation *via* the quinoline π-π* transition at 283 nm (Fig. 21). As the 342 nm emission is also excited by 243 nm absorption, it is concluded that internal energy transfer to the quinolyl group from another locus also occurs. Indeed, ligands **1**–**8** all fluoresce except for ligand **3**. The observed fluorescence for ligand **2** at 362 nm (λ_{ex} 241 nm), for ligand **4** at 365 nm (λ_{ex} 251 nm), for ligand **5** at 362 nm (λ_{ex} 285 nm), for ligand **6** at 356 nm (λ_{ex} 320 nm), and for

Table 2

UV spectroscopic data for ligands **1–8**.

L1 (30.8 μM)		L2 (34.2 μM)		L3 (79.1 μM)		L4 (70.4 μM)		L5 (73.1 μM)	
$\lambda_{max, nm}$	10^{-3} ε, (M^{-1} cm^{-1})	$\lambda_{max, nm}$	10^{-3} ε, (M^{-1} cm^{-1})	$\lambda_{max, nm}$	10^{-3} ε, (M^{-1} cm^{-1})	$\lambda_{max, nm}$	10^{-3} ε, (M^{-1} cm^{-1})	$\lambda_{max, nm}$	10^{-3} ε, (M^{-1} cm^{-1})
207	35.9	208	34.2	203	9.4	208	24.9	212	28.1
215	33.1	215	32.1	261	8.2	248	19.6	263	19.3
241	17.3	228	20.8			298	4.2	283	10.5
266	20.8	236	8.21			309	6.9	292	7.4
285	11.8	335	7.42			331	8.2	322	7.8
321	7.6	348	6.40			343	8.8	334	8.3
333	6.4								

L6 (44.3 μM)		L7 (20.1 μM)		L8 (42.5 μM)		L9 (42.1 μM)	
$\lambda_{max, nm}$	10^{-3} ε, (M^{-1} cm^{-1})	$\lambda_{max, nm}$	10^{-3} ε, (M^{-1} cm^{-1})	$\lambda_{max, nm}$	10^{-3} ε, (M^{-1} cm^{-1})	$\lambda_{max, nm}$	10^{-3} ε, (M^{-1} cm^{-1})
212	37.2	207	28.4	210	42.5	202	53.6
225	25.0	211	24.7	263	31.2	222	15.6
258	22.2	252	14.7	284	10.6	278	9.8
280	7.2	279	14.1	317	7.9	329	8.5
315	5.8			331	7.8	348	10.4
326	5.1					367	10.9
						390	6.3

Table 3

UV spectroscopic data for ligands **9–18**.

L10 (45.9 μM)		L11 (41.2 μM)		L13 (39.3 μM)		L14 (36.6 μM)	
$\lambda_{max, nm}$	10^{-3} ε, (M^{-1} cm^{-1})	$\lambda_{max, nm}$	10^{-3} ε, (M^{-1} cm^{-1})	$\lambda_{max, nm}$	10^{-3} ε, (M^{-1} cm^{-1})	$\lambda_{max, nm}$	10^{-3} ε, (M^{-1} cm^{-1})
202	49.8	205	16.8	207	77.6	208	62.2
228	13.2	222	4.6	211	74.1	214	71.9
276	11.1	261	0.7	245	21.2	251	20.6
329	12.2	274	0.6	249	21.4	256	22.1
347	11.6	282	0.7	269	16.1	271	17.1
367	7.81	291	0.8	276	23.5	278	19.5
391	6.5			283	25.1	286	17.3

L15 (39.1 μM)		L16 (36.2 μM)		L17 (43.1 μM)		L18 (43.1 μM)	
$\lambda_{max, nm}$	10^{-3} ε, (M^{-1} cm^{-1})	$\lambda_{max, nm}$	10^{-3} ε, (M^{-1} cm^{-1})	$\lambda_{max, nm}$	10^{-3} ε, (M^{-1} cm^{-1})	$\lambda_{max, nm}$	10^{-3} ε, (M^{-1} cm^{-1})
206	56.6	208	62.5	208	68.3	205	133
212	72.7	213	70.2	220	92.4	247	222
253	25.3	252	20.9	256	17.1	255	27.2
257	22.2	257	24.4	272	18.8	276	16.5
269	22.1	271	18.1	278	20.4	350	14.1
278	20.2	278	19.4	285	19.3	368	16.3
286	17.4	287	16.7	292	8.7	387	15.2

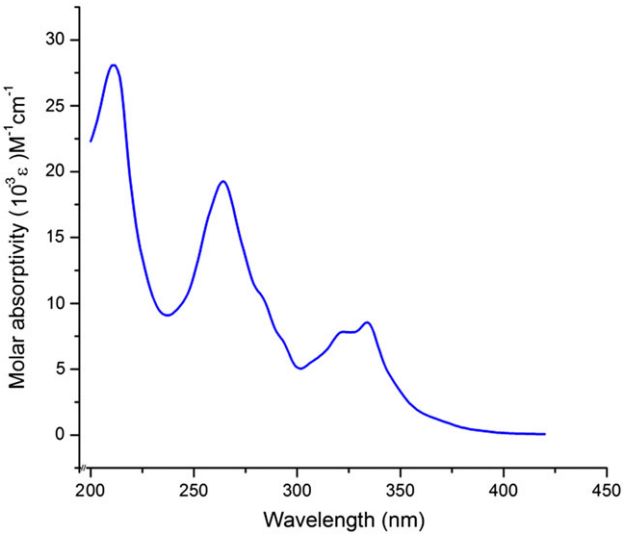

Figure 19. UV spectrum of the quinolyl–tetrahydroindazole ligand **5** (73 μM in acetonitrile). [Color figure can be viewed at wileyonlinelibrary.com]

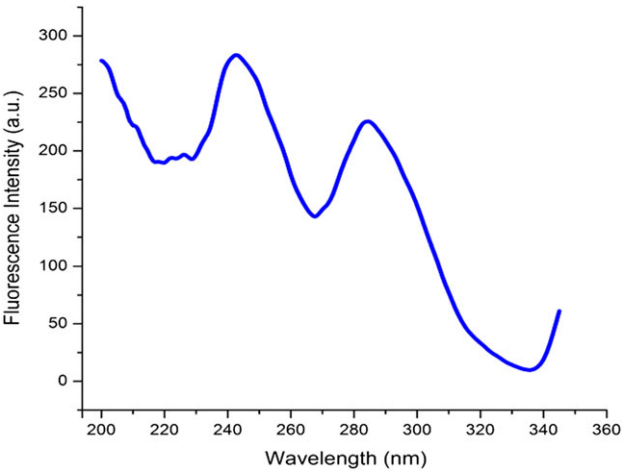

Figure 20. Excitation spectrum of the quinolyl–tetrahydroindazole ligand **1** (1.2 μM) in nonpurged acetonitrile at ambient temperature, from 200 to 345 nm with emission monitored at 350 nm. The ordinate units are arbitrary. [Color figure can be viewed at wileyonlinelibrary.com]

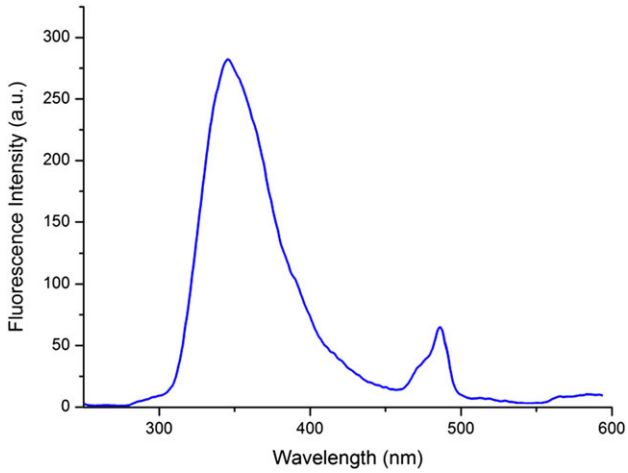

Figure 21. Emission spectrum of the quinolyl–tetrahydroindazole ligand **1** (1.2 μM) in nonpurged acetonitrile at ambient temperature, excited at 240 nm. The feature near 480 nm is a grating ghost. The ordinate units are arbitrary. [Color figure can be viewed at wileyonlinelibrary.com]

Table 4

Maximum absorption (λ_{abs}), excitation wavelength (λ_{ex}), and fluorescence wavelengths (λ_{em}) for ligands in acetonitrile at ambient temperature.

Compound	Absorption maximum (λ_{abs}) nm	Excitation maximum (λ_{ex}) nm	Emission maximum (λ_{em}) nm
1	241	243	342
2	236	241	362
4	248	251	365
5	283	285	362
6	315	320	356
7	256	256	332
8	207	211	348
9	210	212	364
12	222	226	303
13	207	211	305
14	251	257	304
15	257	263	302
16	252	257	300
17	256	258	300
18	255	250	415

ligand **8** at 364 nm (λ_{ex} 212 nm) are attributed to quinoline moiety excitation. Among these fluorescent compounds, the emission observed at 348 nm (λ_{ex} 211 nm) for ligand **7** is assigned to excitation of the pyridine π-π* transition, the large shift to the emission wavelength notwithstanding [45]. The results are summarized in Table 4. It is known that extended system conjugation has a large influence on peak wavelengths and absorption intensities; for instance, benzene, naphthalene, and anthracene display peaks at λ_{max} 255, 286, and 375 nm, respectively. This phenomenon is observed in UV studies of the substituted NTBs, where Np_3NTB and An_3NTB (anthracenylmethyl-NTB) show naphthyl and anthracenyl motifs' absorptions at λ_{max} 286 and 375 nm, respectively. These *N*-alkylated NTB ligands exhibit strong emission at λ_{max} ~300, 330, and 415 nm corresponding to benzene (in benzimidazole), naphthalene, and anthracene motifs' π-π* transitions.

CONCLUSION

Several new metal-chelating compounds with pyrazole, pyridine, quinoline, isoindoline, and phenol donor moieties have been prepared. Straightforward methods such as (a) benzimidazole *N*-alkylation utilizing sodium

metal, (b) addition of arylamines to phthalonitrile, and especially (c) Knorr pyrazole synthesis *via* condensation of arylhydrazine with β-diketone gave successful outcomes. The great majority of these ligands' structures and conformations have been elucidated by X-ray crystallography. The crystallographic approach is structurally definitive for Knorr condensation products with unsymmetric β-diketones, and for one of the compounds described, serves as a strong support for the previously proposed isomer assignment based on ^{13}C NMR [31,32]. The UV absorption and fluorescence spectra have been obtained for the compounds, from which these ligands will find application in the chemistry of luminescent metal chelates.

EXPERIMENTAL

Materials. Reagents (Alfa Aesar, Aldrich, Frinton Laboratories, TCI, Strem) were used as received. UV and luminescence spectra were obtained using PerkinElmer Lambda 35 and 950 UV-Vis spectrophotometers and a PerkinElmer LS55 luminescence spectrophotometer, respectively. FT-IR was obtained on a PerkinElmer Spectrum One instrument. Proton NMR spectra were obtained at room temperature using Varian Unity Inova 300 and 500 MHz spectrometers, with samples in $CDCl_3$ or DMSO-d_6 and TMS as an internal standard. Elemental microanalyses were performed by Robertson-Microlit Laboratories (Ledgewood, NJ) and at the Pisarzhevskii Institute of the NASU. Optical rotation was measured on a PerkinElmer 343 digital polarimeter and CD spectra on a Jasco J-810-150S spectropolarimeter purged with nitrogen; spectra were recorded between 200 and 400 nm with a 500 nm/min scan speed, 1 s response time, 0.05 data pitch and a 5 nm bandwidth; the temperature (23°C) was controlled using a Jasco **(J-810)** Peltier controller (model PTC-423S). Samples were in a 100 μm cell from International Crystal Laboratories. X-ray crystallography was performed at Youngstown State University, Keene State College, and Temple University on Bruker AXS SMART APEX CCD, Rigaku, Oxford diffraction, and Bruker KAPPA APEX II DUO diffractometers using *CrysAlis PRO* 1.171.38.43f (Rigaku), Apex2 v2013.4–1 (Bruker), *SAINT* V8.30C(Bruker), *ShelXT* [46], *SHELXL* [47], *SHELXS97* [48], Olex2 [49], and Olex2. refine [50] programs. Structures were rendered using the ORTEP output mode of the CCDC Mercury 3.9 software. EI-, CI-, APCI-, ESI-, FAB-LSIMS-, and FT-mass spectrometries were performed on Thermo Finnigan TSQ70, Thermo-Electron LTQ-FT 7T, VG70SE, and Sciex API3000 mass spectrometers. A GoldStar MA795W microwave oven was used as microwave reactor.

Preparation of compounds. ***2-(3-Phenyl-4,5,6,7-tetrahydro-2H-indazol-2-yl)quinoline (L1).*** 2-Benzoylcyclohexanone (12.75 mmole, 2.58 g) and 2-hydrazinoquinoline (12.75 mmole, 2.03 g) were refluxed in 125 mL of ethanol for 24 h. The solvent was evaporated to dryness, leaving an amber oil. The oil, in a salt-ice bath, was triturated in the presence of ethanol to yield a brown solid that was then recrystallized from MeOH (charcoaled); crystals were obtained suitable for X-ray diffraction; white solid; yield: 75%; M.p. 94–96°C; ^1H NMR 500 (DMSO-d_6): δ 8.46 (2 H, m), 8.02 (3 H, m), 7.63 (3 H, m), 7.18 (3 H, m), 2.83 (2 H, m), 1.83 (6 H, m); IR (cm^{-1}): 3061, 2922, 1616, 1598, 1492, 1395, 1324, 1250, 1102, 1055, 924, 846, 735; FAB-MS: m/z 326.166, Calcd. for $(M + 1)^+$, 326.165; *Anal*. Calcd. for $C_{22}H_{19}N_3$. 0.5 CH_3OH: C, 78.2; H, 6.27; N, 12.2; found: C, 78.2; H, 5.97; N, 12.0.

2-(3,5-Diphenyl-1H-pyrazol-1-yl)quinoline (L2). Dibenzoylmethane (3.14 mmole, 0.70 g) and 2-hydrazinoquinoline (3.14 mmole, 0.50 g) were refluxed in 125 mL of ethanol for 24 h. The solvent was evaporated to dryness, leaving a dark orange oil. The oil, in a salt-ice bath, was triturated in the presence of ethanol to yield an orange solid that was then recrystallized from MeOH (charcoaled) crystals were obtained suitable for X-ray diffraction; white solid; yield: 92%; M.p. 121–124°C; ^1H NMR 500 ($CDCl_3$): δ 8.10 (4H, d, J = 8.24), 7.84 (3H, d, J = 8.62), 7.50 (3H, m), 7.35 (6H, m), 6.9 (1 H, s); IR (cm^{-1}): 3062, 2922, 1616, 1600, 1570, 1488, 1407, 1350, 1260, 1125, 1077, 954, 829, 754; FAB-MS: m/z 348.150, Calcd. for $(M + 1)^+$, 348.150; *Anal*. Calcd. for $C_{24}H_{17}N_3$. 1 H_2O: C, 78.9; H, 5.24; N, 11.5: found: C, 78.6; H, 5.27; N, 11.2.

(4S,7S)-7,8,8-Trimethyl-1-(pyridin-2-yl)-4,5,6,7-tetrahydro-1H-4,7-methanoindazole (L3). L3 was prepared by refluxing 0.721 g (4.0 mmol) of 3-(hydroxymethylene) camphor and 0.463 g (4 mmol) 2-hydrazinopyridine in 50 mL of ethanol for 2.5 days. The solvent was removed at the rotary evaporator and the ligand was recrystallized from chloroform (charcoaled); crystals were obtained suitable for X-ray diffraction; white solid; yield: 72%; M. p. 160–162°C; ^1H NMR 500 (DMSO-d_6) δ 7.72 (m, 1H), 7.48 (m, 2H), 7.38 (m, 1H), 2.18 (m, 1H), 1.92 (m, 1H), 1.24 (m, 3H), 0.96 (m, 6H), 0.72 (m, 3H); IR (cm^{-1}): 3054, 2953, 1611, 1592, 1512, 1436, 1386, 1111, 1020, 985, 910, 761, 688. *Anal*. Calcd. for $C_{16}H_{19}N_3$, C, 75.8, H, 7.56, N, 16.6; found, C, 76.0, H, 7.21, N, 16.4; APCI-MS: m/z 253.158, Calcd. for (M^+), 253.157.

2-(3-Methyl-1H-indazol-1-yl)quinoline (L4). 2′-fluoroacetophenone (21 mmole, 2.90 g) and 2-hydrazinoquinoline (21 mmole, 3.34 g) were refluxed in ethylene glycol for 24 h. The solution was cooled and water was added to precipitate a finely divided brown solid, which was filtered off and recrystallized from

MeOH (charcoaled); crystals were obtained suitable for X-ray diffraction; brown solid; yield: 55%; M.p. 107–110°C; ^{1}H NMR 500 (DMSO- d_6): δ 9.11 (d, 1H, J = 8.45), 8.52 (d, 1H, J = 8.96), 8.25 (d, 1H J = 8.96), 8.09 (d, 1H, J = 8.20), 8.01 (d, 1H, J = 8.00), 7.89 (d, 1H, J = 7.95), 7.81 (t, 1H, J = 7.64), 7.67 (t, 1H, J = 7.70), 7.58 (t, 1H, J = 7.45), 7.38 (t, 1H, J = 7.46), 2.62 (s, 3); IR (cm^{-1}): 3051, 2916, 1620, 1599, 1433, 1397, 1339, 1217, 1084, 823, 737; FAB-MS: m/z 260.118, Calcd. for (M + 1)$^+$, 260.118; *Anal*., calculated for $C_{17}H_{13}N_3$: C, 78.7; H, 5.05; N, 16.2. Found: C, 78.7; H, 5.42; N, 16.3.

2-(3-Methyl-4,5,6,7-tetrahydro-2H-indazol-2-yl)quinoline (L5). A sample of 2-acetylcyclohexanone (1.7 mmole, 0.27 g) and 2-hydrazinoquinoline (1.7 mmole, 0.24 g) were refluxed in iPrOH, for 2 days, the reaction mixture rotavapored down to dryness, resulting a brown oil residue from which a white power was obtained through recrystallization from MeOH (charcoaled); crystals were obtained suitable for X-ray diffraction; white solid; yield: 65%; M.p. 110–112°C; ^{1}H NMR 500 ($CDCl_3$): δ 8.22 (1 H, d, J = 8.75), 8.09 (1 H, d, J = 8.59), 7.90 (1 H, d, J = 7.28), 7.80 (1 H, d, J = 8.25), 7.68 (1 H, t, J = 7.34), 7.48 (1 H, t, J = 6.68), 2.76 (4 H, m), 2.52 (2 H, m), 1.82 (5 H, m); IR (cm^{-1}): 3055, 2921, 1616, 1600, 1502, 1422, 1367, 1049, 954, 829, 756; CI-MS: m/z 263.141, Calcd. for (M$^+$), 263.142; *Anal*., calculated for $C_{17}H_{17}N_3$: C, 77.5; H, 6.51; N, 16.0. Found: C, 77.6; H, 6.54; N, 15.9.

2-(3,5-Di-tert-butyl-1H-pyrazol-1-yl)quinolone (L6). **L6** was prepared by refluxing 1.33 mL (6.37 mmol) of 2,2,6,6-tetramethyl-2,5-heptanedione and 1.01 g (6.37 mmol) of 2-hydrazinoquinoline in 30 mL of ethylene glycol for 24 h. The solution was cooled to room temperature, water was added to the reaction mixture, until a precipitate was obtained. The crude ligand recrystallized from MeOH (charcoaled); crystals were obtained suitable for X-ray diffraction; yellow solid; yield: 86%; M.p. 134–137°C; ^{1}H NMR 500 (DMSO-d_6): δ 8.58 (1 H, d, J = 8.60), 8.09 (1 H, d, J = 8.26), 7.98 (1 H, d, J = 8.48), 7.84 (1 H, t, J = 7.63), 7.76 (1 H, d, J = 8.65), 7.68 (1 H, t, J = 7.38), 6.28 (1 H, s), 1.36 (9 H, s), 1.28 (9 H, s); IR (cm^{-1}): 3049, 2958, 1618, 1597, 1502, 1440, 1358, 1245, 1015, 994, 835, 762; CI-MS: m/z 308.213, Cacld. for (M + 1)$^+$, 308.212; *Anal*. Calcd. for $C_{20}H_{25}N_3$. 0.25 CH_3OH: C, 77.1; H, 8.31; N, 13.3; found, C, 77.4; H, 7.92; N, 13.5.

2-(3-Methyl-1-(pyridin-2-yl)-1H-pyrazol-5-yl)phenol (L7). Salicyloylacetone (2.0 mmole, 0.36 g, Frinton) and 2-hydrazinopyridine (2.0 mmole, 0.22 g) were refluxed in EtOH for 3 days, after which the product was filtered off from the cooled solution, and recrystallized from MeCN (charcoaled); crystals were obtained suitable for X-ray diffraction; yellow solid; yield: 82%, M.p. 154–156°C; ^{1}H NMR 500 (DMSO-d_6): δ 9.32 (1 H, d, J = 6.81), 8.21 (1 H, d, J = 6.22), 7.94 (1 H, t, J = 7.81), 7.64 (1 H, m), 7.12–7.34 (2 H, m), 6.72–6.92 (3 H, m), 6.34 (1 H, m), 2.32 (3 H, m); IR (cm^{-1}): 3400, 3060, 2940, 1594, 1570, 1550, 1465, 1440, 1363, 1210, 1097, 982, 850; CI-MS: m/z 252.112, Calcd. for (M + 1)$^+$, 252.113; $C_{15}H_{13}N_3O{\cdot}1H_2O$: C, 66.9; H, 5.61; N, 15.6. Found: C, 66.6; H, 5.51; N, 15.6.

2-(3-Methyl-1-(quinolin-2-yl)-1H-pyrazol-5-yl)phenol (L8). Salicyloylacetone (2.5 mmole, 0.45 g) and 2-hydrazinoquinoline (2.5 mmole, 0.40 g) were refluxed in EtOH for 3 days, the solution was cooled down, filtered off, and recrystallized from MeCN (charcoaled); crystals were obtained suitable for X-ray diffraction; white solid; yield: 63%, M.p. 209–211°C; ^{1}H NMR 500 (DMSO-d_6): δ 9.22 (1 H, s), 8.42 (1 H, d, J = 8.84), 7.96 (1 H, d, J = 8.08), 7.86 (1 H, t, J = 7.70), 7.64 (1 H, t, J = 7.65), 7.52 (1 H, t, J = 7.50), 7.32 (1 H, d, J = 8.40), 7.26 (1 H, d, J = 7.48), 7.18 (1 H, m), 6.88 (1 H, t, J = 7.45), 6.68 (1 H, d, J = 8.11), 6.34 (1 H, s), 2.36 (3 H, s). IR (cm^{-1}): 3350, 3090, 2935, 1598, 1550, 1480, 1447, 1379, 1267, 1184, 1108, 944, 827, 790, 765, 755; APCI-MS: m/z 302.128, Calcd. for (M + 1)$^+$, 302.129; $C_{19}H_{15}N_3O{\cdot}1H_2O$: C, 71.5; H, 5.37; N, 13.2. Found: C, 71.3; H, 4.98; N, 13.2.

(1Z,3Z)-N1,N3-bis(5-phenyl-1H-pyrazol-3-yl)isoindoline-1,3-diimine (L9). Pyrazole (0.95 g, 6 mmol) was mixed with phthalonitrile (0.38 g, 3 mmol) in a test tube, which was inserted into an aluminum block on a hotplate, heated to 175°C for 5 h, resulted in deep red mass, which was then dissolved in hot DMF (*N,N*-dimethylformamide), after which water was added to the reaction mixture, until red crystals were obtained, yield: 81%. In the solventless melt method, phthalonitrile was thus simply heated with 3-amino-5-phenylpyrazole, while in the microwave method, ethylene glycol was added as a microwave absorber. Single crystals were grown in NMP; M.p. >220°C; IR (cm^{-1}): 3300, 3060, 1633, 1564, 1482, 1300, 1203, 856, 803, 755. APCI-MS: m/z 430.181, Calcd. for (M + 1)$^+$, 430.180; $C_{26}H_{19}N_7$ 0.5 H_2O: C, 71.2; H, 4.60; N, 22.4: found: C, 71.6; H, 4.25; N, 22.7, ^{1}H NMR 500 (DMSO-d_6): δ 13.34 (2 H, s), 8.01 (6 H, d, J = 7.42), 7.72 (2 H, m), 7.50 (6 H, m), 7.32 (2 H, s), 6.81 (1 H, s).

(1Z,3Z)-N1,N3-bis(5-methyl-1H-pyrazol-3-yl)isoindoline-1,3-diimine (L10). **L10** was prepared by the solventless melt method: 0.38 g (3 mmol) of phthalonitrile fused with 0.95 g (6 mmol) of 3-amino-5-phenylpyrazole for 3 h, 180–190°C gave 1.25 g red crystals of crude product when subsequently digested in hot DMF and ppted. with hot water. Recrystallization from wet DMF (charcoal) gave 0.50 g (40%) golden-buff microcrystals after drying in vacuo at 100°C. Crystals suitable for X-ray diffraction were obtained from DMF; M.p. >220°C; ^{1}H NMR 500 (DMSO-d_6): δ 12.50 (2 H, d, J = 6.38), 11.84 (1 H, d, J = 6.48), 7.98 (2 H, d, J = 5.37), 7.72 (2 H, d, J = 6.52), 6.10 (2 H, d, J = 5.64), 2.32 (6 H, m); IR (cm^{-1}): 3233, 3059, 2985, 1629, 1566, 1213, 1120, 863, 780, 730;

FAB-MS: m/z 306.145, Calcd. for $(M + 1)^+$, 306.146; *Anal*. Calcd. for $C_{16}H_{15}N_7$ 0.25 H_2O: C, 62.0; H, 5.04; N, 31.6: found: C, 62.2; H, 4.93; N, 32.0.

For the microwave method: to phthalonitrile (2.56 g, 20 mmol) and 3-amino-5-methylpyrazole (3.90 g, 40 mmol) in a 50 mL Erlenmeyer flask was added 0.5 mL of ethylene glycol as a microwave absorber. The mixture was microwaved (*ca*. 100 W) until it melted, upon which it was swirled to effect mixing. It was then microwave-pulsed for 30 s periods (100 W) at intervals of 1.5 min, until the now greenish-brown melt ceased evolving ammonia (*ca*. 12 min). Recrystallization was from DMF (charcoal) with water added, giving golden-yellow crystals that were dried in vacuo at 100°C; yield 29%; M.p. >220°C; FAB-MS, $(M + 1)^+$ m/z 306.146.

1,2-Bis(1,4,5,6-tetrahydropyrimidin-2-yl)benzene (L11). **L11** was prepared by the solventless melt method: 0.38 g (3 mmol) of phthalonitrile fused with 0.44 g (6 mmol) of 1,3-diaminopropane for 3 h, 180–190°C product was obtained when digested in hot DMF and ppted. by hot water addition; yellow solid; yield: 58%; M.p. 118–120°C; ^{1}H NMR 500 (DMSO-d_6): δ 8.22 (4 H, m), 8.12–7.90 (4 H, m), 3.42 (8 H, m), 2.62 (4 H, m); IR (cm^{-1}): 3255, 3080, 2920, 1640, 1590, 1484, 1394, 1228, 1206, 965, 806, 769, 719; APCI-MS: m/z 243.161, Calcd. for $(M + 1)^+$, 243.160; *Anal*. Calcd. for $C_{14}H_{18}N_4$: C, 69.4; H, 7.49; N, 23.1: found: C, 69.5; H, 7.10; N, 23.1.

Tris(benzimidazol-2-ylmethyl)amine derivatives (L12–18). Tris(benzimidazol-2-ylmethyl)amine (NTB) **L12** and **L13** were prepared as previously described [51,52]. Alkylation of NTB is exemplified by the preparation of Et_3NTB to 9.82 g (20 mmol) of NTB in 16 mL of DMSO vented and under N_2 was added 0.95 g (41 mmol) of Na-metal. The mixture was stirred until the sodium had dissolved (this may take 6–50 h, depending on the benzimidazole and the temperature). To the now-homogeneous solution was added 4.36 g (40 mmol) of bromoethane, and following an initial mild exothermicity, the reaction mixture was stirred for several hours, after which reaction products had precipitated. The mixture was then diluted with water (20 mL) and benzene (or toluene) (25 mL) and stirred at length to partition the product into the nonaqueous layer. This mixture was then filtered to remove solid impurities; the product was isolated from the benzene/toluene layer by evaporation of the solvent, to yield a straw-colored "honey," which crystallizes if allowed to stand for a long time. Recrystallization from decane (charcoal) gave straw-colored crystals. FAB-MS: m/z 492.288, Calcd. for $(M + 1)^+$, 492.287; *Anal*. Calcd. for $C_{30}H_{33}N_7$, C, 73.3; H, 6.77; N, 19.9: found: C, 73.0; H, 6.75; N, 20.0.

Tris(N1-ethylbenzimidazol-2-ylmethyl)amine (L14). Et_3NTB: white solid; single crystals were grown in MeCN; yield: 71%; M.p. >220°C; ^{1}H NMR 500 (DMSO-d_6): δ 7.72 (3 H, m), 7.52 (3 H, m), 7.26 (6 H, m), 4.26 (6 H, m), 3.72 (6 H, m), 1.02–0.88 (9 H, m). IR (cm^{-1}): 3053, 2974, 1615, 1514, 1165, 1093, 855, 788, 735. FAB-MS: m/z 492.288, Calcd. for $(M + 1)^+$, 492.287; *Anal*. Calcd. for $C_{30}H_{33}N_7$, C, 73.3; H, 6.77; N, 19.9: found: C, 73.0; H, 6.75; N, 20.0.

Tris(N1-n-propylbenzimidazol-2-ylmethyl)amine (L15). Pr_3NTB: white solid; recrystallized (charcoaled) from 1:3 MeCN:$CHCl_3$; yield: 72%, M.p. >220°C; ^{1}H NMR ($CDCl_3$): δ 8.87 (6 H, m), 8.37 (6 H, m), 5.35 (6 H, m), 4.52 (6 H, s), 3.85 (6 H, t, J = 6.72), 2.34 (6 H, m), 1.34 (9 H, t, J = 6.88); IR (cm^{-1}): 3054, 2986, 1616, 1590, 1516, 1460, 1416, 1331, 1250, 1160, 1092, 853, 768, 733; APCI-MS: m/z 534.333, Calcd. for $(M + 1)^+$, 534.334; *Anal*. Calcd. for $C_{33}H_{39}N_7$, C, 74.3; H, 7.37; N, 18.4: found: C, 74.0; H, 7.55; N, 18.0.

Tris(N1-n-butylbenzimidazol-2-ylmethyl)amine (L16). Bu_3NTB; white solid; single crystals were grown from 1:3 MeCN:$CHCl_3$; yield: 78%; M.p. >220°C; ^{1}H NMR ($CDCl_3$): δ 7.77 (6 H, m), 7.24 (6 H, m), 4.25 (6 H, m), 3.43 (12 H, m), 1.15 (6 H, m), 0.51 (9 H, m). IR (cm^{-1}): 3051, 2968, 1620, 1599, 1509, 1460, 1357, 1320, 1286, 1159, 1086, 991, 872, 735. *Anal*. Calcd. for $C_{36}H_{45}N_{7:}$ C, 75.1; H, 7.88; N, 17.0: found: C, 74.6; H, 7.64; N, 17.0; APCI-MS: m/z 576.382, Calcd. for $(M + 1)^+$, 576.381.

Tris(N1-[1′-naphthyl]methylbenzimidazol-2-yl)amine (L17). Np_3NTB, cream solid; single crystals were grown from 1:3 MeCN:$CHCl_3$; yield: 72%; M.p. >220°C; ^{1}H NMR 500 (DMSO-d_6): δ 7.90 (3 H, d, J = 5.75), 7.72(3 H, d, J = 5.93), 7.63(3 H, d, J = 5.35), 7.50 (3 H, m), 7.44 (3 H, m), 7.28 (3 H, m), 7.02 (3 H, m), 6.96 (6 H, m), 6.91 (6 H, m), 5.65 (6 H, m), 4.10 (6 H, s). IR (cm^{-1}): 3053, 2956, 1618, 1540, 1460, 1298, 1223, 1162, 998, 814, 720; APCI-MS: m/z 828.382, Calcd. for $(m + 1)^+$, 828.381; *Anal*. Calcd. for $C_{57}H_{45}N_7$0.3$CHCl_3$: C, 79.7; H, 5.29; N, 11.3; found: C, 79.6; H, 5.43; N, 11.4.

Tris(N1-[9′-anthracenyl]methylbenzimidazol-2-ylmethyl) amine (L18). An_3NTB; yellow solid; recrystallized (charcoaled) from 1:3 MeCN:$CHCl_3$; yield: 65%; M.p. >220°C; ^{1}H NMR 500 (DMSO-d_6): δ 9.18 (3 H, m), 8.59 (6 H, m), 8.45 (3 H, d, J = 6.15), 7.92 (3 H, m), 7.88 (3 H, m), 7.76 (3 H, m), 7.60 (3 H, m), 7.33 (3 H, m), 6.94 (6 H, m), 6.38 (3 H, m), 6.28 (3 H, s), 5.20 (6 H, m), 3.98 (6 H, s). IR (cm^{-1}): 3051, 2950, 1613, 1521, 1502, 1420, 1303, 1211, 1181, 1020, 954, 820, 725; APCI-MS: m/z 978.428, Calcd. for $(M + 1)^+$, 978.429; *Anal*. Calcd. for $C_{69}H_{51}N_7$1CH_3CN·0.6$CHCl_3$: C, 78.8; H, 5.05; N, 10.2; found: C, 78.7; H, 5.08; N, 10.1.

Acknowledgments. The authors thank Drexel University for support, D. DiGuiseppi for assistance with CD, Drs. R.J. Butcher and M.J. Zdilla for assistance with structure files, Dr. D Martinez Solorio for helpful discussion, and Dr. A.V. Pavlishchuk for the Art Museum image. J. P. J. and M. K. acknowledge the NSF–MRI program (grant no. 1039027) for funds to purchase the

X-ray diffractometer, while M. Z. acknowledges NSF-DMR (1337296), CHE (0087210), and Ohio Board of Regents (grant CAP-491) for diffractometer funding.

REFERENCES AND NOTES

[1] Gray, H. B PNAS 2003, 100, 7, 3563.
[2] Glusker, J. P.; Katz, A. K.; Bock, C. W. The Rigaku Journal 1999, 16, 8.
[3] Seleem, H. S. Chem Cent J 2011, 5, 35.
[4] Chetia, B.; Iyer, P. K. Tetrahedron Lett 2007, 48, 47.
[5] Ghosha, K.; Adhikari, S.; Fröhlich, R. Tetrahedron Lett 2008, 49, 5063.
[6] Addison, A. W.; Burke, P. J. J Heterocyclic Chem 1981, 18, 803.
[7] Addison, A. W.; Rao, T. N.; Wahlgren, C. G. J Heterocyclic Chem 1983, 20, 1481.
[8] Wahlgren, C. G.; Addison, A. W. J Heterocyclic Chem 1989, 26, 541.
[9] Gilbert, J. G.; Addison, A. W.; Palaniandavar, M.; Butcher, R. J. J Heterocyclic Chem 2002, 39, 2, 399.
[10] Dagdigian, J. V.; Reed, C. A Inorg Chem 2623, 1979(18), 9.
[11] Freire, E.; Baggio, S.; Munoz, J. C.; Baggio, R. Acta Crystallogr 2003, C59, o259.
[12] Amrutkar, S. V.; Sunil, V.; Bhagat, U. D.; Pargharmol, P.; Kotgire, S. S. Int J Pharm Sci 2010, 2, 84.
[13] Vaidya, S. D.; Kumara, B. V. S.; Kumar, U. N. J Heterocyclic Chem 2007, 44, 685.
[14] Nassar, E. M.; El-Farargy, A. E.; Abdelrazek, F. M. J Heterocyclic Chem 2015, 52, 1395.
[15] Starcevic, K.; Kralj, M.; Ester, K.; Sabol, I.; Grce, M.; Pavelic, K.; Karminski-Zamola, G. Bioorg Med Chem 2007, 15, 4419.
[16] Galal, S. A.; Hageb, K. H.; Kassab, A. S.; Rodriguez, M. L.; Kerwin, S. M.; El-Khamry, A. A.; El Diwani, H. I. Eur J Med Chem 2009, 44, 1500.
[17] Keller, P.; Müller, C.; Engelhardt, I.; Hiller, E.; Lemuth, K.; Eickhoff, H.; Wiesmüller, K.-H.; Burger-Kentischer, A.; Bracher, F.; Rupp, S. Antimicrob Agents Chemother 2015, 59, 6296.
[18] Bai, Y.-B.; Zhang, A.-L.; Tang, J.-J.; Gao, J.-M. J Agric Food Chem 2013, 61, 2789.
[19] Taylor, R. D.; MacCoss, M.; Lawson, A. D. G. J Med Chem 2014, 57, 5845.
[20] Su, C.-Y.; Kang, B.-S.; Du, C.-X.; Yang, Q.-C.; Mak, T. C. W Inorg Chem 2000, 39, 4843.
[21] Gregorzik, R.; Hartmann, U.; Vahrenkamp, H. Ber Dtsch Chem Ges 1994, 127, 2117.
[22] Addison, A. W.; Henriks, H.; Reedijk, J.; Thompson, L. K. Inorg Chem 1981, 20, 103.
[23] Chen, B.-T.; Morlanés, N.; Adogla, E.; Takanabe, K.; Rodionov, V. O ACS Catal 2016, 6, 4647.
[24] Yan, C.; Li, K.; Wei, S.-C.; Wang, H.-P.; Fu, L.; Pan, M.; Su, C.-Y. J Mater Chem 2012, 22, 9846.
[25] Pan, M.; Lan, M.-H.; Wang, X.-T.; Yan, C.; Liu, Y.; Su, C.-Y. Inorg Chim Acta 2010, 363, 3757.
[26] Wu, H.; Bai, Y.; Wang, X.; Zhang, Y.; Shi, F.; Bai, Y.; Pan, G.; Kong, J. Transition Met Chem 2013, 38, 553.
[27] Wu, H.; Bai, Y.; Jingkun, Y.; Wang, H.; Pan, G.; Fan, X.; Kong, J. J Chem Res 2012, 36, 283.
[28] Sinha, S.; Berdichevsky, E. K.; Warren, J. J. Inorg Chim Acta 2017, 460, 63.
[29] Stott, L. A.; Prosser, K. E.; Berdichevsky, E. K.; Walsby, C. J.; Warren, J. J C Chem Commun 2017, 53, 651.
[30] Knorr, L. Ber Dtsch Chem Ges 1883, 16, 2597.
[31] Catalan, J.; Fabero, F.; Claramunt, R. M.; Santa Maria, M. D.; Foces, M. C.; Cano, F. H.; Martinez-Ripoll, M.; Elguro, J.; Sastre, R. J Am Chem Soc 1992, 114, 5039.
[32] Singh, S. P.; Kumar, D.; Kumar, D. Synth Commun 1996, 26, 3193.
[33] Elguero, J.; Martinez, A.; Singh, S. P.; Grover, M.; Tarar, L. S. J Heterocyclic Chem 1990, 27, 865.
[34] Khan, M. A.; Polya, J. B. J Chem Soc (C) 1970 85.
[35] Bernal, I. Inorg Chim Acta 1985, 96, 99.
[36] Wu, T.; You, X. J Phys Chem A 2012, 116, 8959.
[37] Saeed, A.; Ejaz, S. A.; Shehzad, M.; Hassan, S.; al-Rashida, M.; Lecka, J.; Sevigny, J.; Iqbal, J. RSC Adv 2016, 25, 21026.
[38] Elvidge, J. A.; Linstead, R. P. J Chem Soc 1952 5000.
[39] Siegl, W. O. J Org Chem 1977, 42, 1872.
[40] Lever, A. B. P.; Ramaswamy, B. S.; Simonse, S. H.; Thompson, L. K. Can J Chem 1970, 48, 3076.
[41] Nozari, M.; Addison, A. W.; Zeller, M. Chem Abstr 2014 1303793.
[42] Smith, V. I.; Nozari, M.; Zeller, M.; Addison, A. W. Acta Crystallogr 2017, E73, 127.
[43] Snyder, R.; Testa, A. C. J Phys Chem 1984, 88, 5948.
[44] Bernarducci, E.; Schwindinger, W. F.; Hughey, J. L. IV; Jesperson, K. K.; Schugar, H. J. J Am Chem Soc 1981, 103, 1686.
[45] Yamazaki, I.; Sushida, K.; Baba, H. J Chem Phys 1979, 71, 381.
[46] Sheldrick, G. M. Acta Crystallogr 2015, A71, 3.
[47] Sheldrick, G. M. Acta Crystallogr 2015, C71, 3.
[48] Sheldrick, G. M. Acta Crystallogr 2008, A64, 112.
[49] Dolomanov, O. V.; Bourhis, L. J.; Gildea, R. J.; Howard, J. A. K.; Puschmann, H. J Appl Cryst 2009, 42, 339.
[50] Bourhis, L. J.; Dolomanov, O. V.; Gildea, R. J.; Howard, J. A. K.; Puschmann, H. Acta Crystallogr 2015, A71, 59.
[51] Thompson, L. K.; Ramaswamy, B. S.; Seymour, E. A. Can J Chem 1977, 55, 878.
[52] Hendriks, H. M. J.; Birker, P. J. M. W. L.; Verschoor, G. C.; Reedijk, J. J Chem Soc Dalton Trans 1982 623.

SUPPORTING INFORMATION

Additional Supporting Information may be found online in the supporting information tab for this article.